

Extraction of proton form factors in the timelike region from single-polarized $e^+e^- \rightarrow \vec{p}\bar{p}$ events

Andrea Bianconi*

*Dipartimento di Chimica e Fisica per i Materiali e per l'Ingegneria,
via Valotti 9, 25100 Brescia, Italy, and*

Istituto Nazionale di Fisica Nucleare, Sezione di Pavia, I-27100 Pavia, Italy

Barbara Pasquini[†] and Marco Radici[‡]

Dipartimento di Fisica Nucleare e Teorica, Università di Pavia, and

Istituto Nazionale di Fisica Nucleare, Sezione di Pavia, I-27100 Pavia, Italy

We have performed numerical simulations of the single-polarized $e^+e^- \rightarrow \vec{p}\bar{p}$ process in kinematic conditions under discussion for a possible upgrade of the existing DAFNE facility. By fitting the cross section and spin asymmetry angular distributions with typical Born expressions, we can study the conditions for extracting information on moduli and phases of the proton electromagnetic form factors in the timelike region, which are poorly known and whose preliminary data show puzzling features. We have explored also non-Born contributions by introducing a further component in the angular fit, which is related to two-photon exchange diagrams. Using a dipole parametrization, we show that these corrections can be identified if larger than 5% of the Born contribution; we also explore the conditions for extracting information on the phase and, consequently, on the relative weight between their real and imaginary parts, which are presently unknown.

PACS numbers: 13.66.Bc, 13.40.Gp, 13.40.-f, 13.88.+e

*Electronic address: andrea.bianconi@bs.infn.it

[†]Electronic address: barbara.pasquini@pv.infn.it

[‡]Electronic address: marco.radici@pv.infn.it

I. INTRODUCTION

The electromagnetic form factors are one of the most relevant sources of information on the structure of hadrons and on their internal quark/gluon dynamics. A lot of data for nucleons have been accumulated in the spacelike region using elastic electron scattering (for a review, see Ref. [1] and references therein). While the traditional Rosenbluth separation method suggests the well known scaling of the ratio G_E/G_M of the electric to the magnetic Sachs form factor, new measurements on the electron-to-proton polarization transfer in $\vec{e}^- p \rightarrow e^- \vec{p}$ scattering reveal contradicting results, with a monotonically decreasing ratio for increasing momentum transfer $-q^2 = Q^2$ [2]. This has led to several theoretical works in order to test the reliability of the Born approximation underlying the Rosenbluth method (see Ref. [3] and references therein).

Hadron form factors are experimentally less well known in the timelike region $q^2 > 0$, where they can be explored in e^+e^- annihilations or hadron-hadron collisions (for a review see Ref. [4]). Being complex objects, their absolute values can be extracted by combining the measurement of total cross sections and center-of-mass (c.m.) angular distributions of the final products. The phases are related to the polarization of the involved hadrons (see, e.g., Refs. [4, 5, 6]), but they have not yet been measured. The available unpolarized differential cross sections have always been integrated over a wide angular range, such that the relative weight of $|G_M|$ and $|G_E|$ is still unknown. In the data analysis either hypothesis $G_E = 0$ or $|G_E| = |G_M|$ were used for all q^2 , which are both not justified *a priori*.

Nevertheless, the few available results show quite interesting properties. The amplitudes in the timelike and spacelike regions are connected by dispersion relations [7]; consequently, at sufficiently large $|q^2|$ the form factors should behave in a similar way in both regions. A fit to the existing proton $|G_M|$ data for $q^2 \leq 20$ GeV 2 [8] suggests that surprisingly this asymptotic regime has not yet been reached. Moreover, the very recent data from the BaBar collaboration on $|G_E/G_M|$ [9] show that the ratio is larger than 1, contradicting the spacelike results with the polarization transfer method [2] and the previous timelike data from LEAR [10]. Also the few neutron $|G_M|$ data are unexpectedly larger than the proton ones in the corresponding q^2 range [11]. Finally, very close to the threshold $q^2 = 4m^2$ (with m the nucleon mass), the trend of data suggests that the form factors could be affected by interesting subthreshold resonance structures (for more details, see Ref. [12]).

The ongoing discussion about the upgrade of the DAFNE facility [13] by enlarging the c.m. energy range from the ϕ mass to 2.5 GeV while keeping a luminosity of $10^{32} \text{ cm}^{-2}\text{s}^{-1}$, and, in particular, by inserting a polarimeter around the interaction region [14], would allow to explore the production of polarized $p\bar{p}$, $n\bar{n}$, $\Lambda\bar{\Lambda}$, and $\Sigma\bar{\Sigma}$ pairs with great precision. As for protons, in a previous paper [15] we explored the conditions under which the ratio $|G_E/G_M|$ could be extracted at DAFNE-2 from the angular distribution of the unpolarized cross section at any given q^2 . We showed that with 300 000 events in the considered $3.8 \leq q^2 \leq 6.2 \text{ GeV}^2$ region, the uncertainty on the ratio is about 10%. Here, we consider the case where the final proton is polarized normally to the reaction plane. Using the same sample of events, we try to determine the conditions to realistically extract the phase of G_E/G_M from the simulation of a single-spin asymmetry measurement.

We also made some simulations of non-Born contributions, mainly related to two-photon (2γ) exchange diagrams, which seem to play a crucial role in the analysis of the G_E/G_M ratio in the spacelike region [2]. Theoretically, these mechanisms are very poorly known; in particular, the relative size of the real and imaginary parts is undetermined. Therefore, in our simulations we explore the most favourable conditions to set upper limits on their magnitude and verify if their contribution can be measured at DAFNE-2. In Ref. [15], we assumed the 2γ amplitude mainly real, and we came to the preliminary conclusion that their effect can be isolated only if their absolute size is at least 5% of the Born contribution. Here, at variance, we check that if the 2γ amplitude is mainly imaginary, its effect could be detected more easily in single-spin asymmetries than from unpolarized cross sections.

In Sec. II, we briefly review the necessary general formalism. In Sec. III, we outline the main features of our Monte Carlo simulation of the $e^+e^- \rightarrow \vec{p}\bar{p}$ process. In Sec. IV, we describe the steps to extract information on form factors by reconstructing the simulated normal polarization with a two-parameter fit. In Sec. V, we discuss the results. Finally, some concluding remarks are given in Sec. VI

II. GENERAL FORMALISM

The scattering amplitude for the reaction $e^+e^- \rightarrow p\bar{p}$, where an electron and a positron with momenta k_1 and k_2 , respectively, annihilate into a proton-antiproton pair with momenta p_1 and p_2 , respectively, is related by crossing to the corresponding scattering amplitude for

elastic e^-p scattering. There are several equivalent representations of it; here, we use the one involving the axial current following the scheme of Ref. [16]. The scattering amplitude can be fully parametrized in terms of three complex form factors: $G_E(q^2, t)$, $G_M(q^2, t)$, and $G_A(q^2, t)$, which are functions of $q^2 = (k_1 + k_2)^2$ and $t = (k_2 - p_1)^2$. They refer to an identified proton-antiproton pair in the final state, rather than to an identified isospin state. In the following, we will use $\cos \theta$ instead of the variable t , with θ the angle between the momenta of the positron and of the recoil proton in the c.m. frame.

In the Born approximation, G_E and G_M reduce to the usual Sachs form factors and do not depend on $\cos \theta$, while $G_A = 0$. For the construction of our Monte Carlo event generator, we rely on the general and extensive relations of Ref. [16] up to the single polarization case. These relations assume small non-Born terms and include them up to order α^3 (with α the fine structure constant), i.e. they consider 2γ exchanges only via their interference with the Born amplitude. These corrections introduce explicitly six new functions that all can depend on $\cos \theta$: the real and imaginary parts of ΔG_E and ΔG_M , i.e. of the 2γ corrections to the Born magnetic and electric form factors, and the real and imaginary parts of the axial form factor G_A .

The role of these corrections in the unpolarized and single-polarized cross sections is very simple: it can be deduced from the Born term by adding the contribution of G_A and substituting the Born form factors with the "2 γ -improved" ones, i.e. $G_{E,M}(q^2) \rightarrow G_{E,M}(q^2) + \Delta G_{E,M}(q^2, \cos \theta)$. In Ref. [16], this fact is somehow hidden by neglecting terms of order α^4 . For sake of simplicity, we keep 2γ effects via the axial form factor only. Within this scheme, when summing events with positive and negative polarization, the unpolarized cross section can be written as

$$\frac{d\sigma^o}{d\cos \theta} = a(q^2) [1 + R(q^2) \cos^2 \theta] - b(q^2) \operatorname{Re}[G_M(q^2) G_A^*(q^2, \cos \theta)] \cos \theta, \quad (1)$$

$$a(q^2) = \frac{\alpha^2 \pi}{2q^2} \frac{1}{\tau} \sqrt{1 - \frac{1}{\tau}} \left(\tau |G_M|^2 + |G_E|^2 \right), \quad b(q^2) = \frac{2\pi\alpha^2}{q^2} \frac{\tau - 1}{\tau}, \quad (2)$$

$$R(q^2) = \frac{\tau |G_M(q^2)|^2 - |G_E(q^2)|^2}{\tau |G_M(q^2)|^2 + |G_E(q^2)|^2}, \quad \tau = \frac{q^2}{4m^2}. \quad (3)$$

When the proton is polarized, the cross section is linear in the spin, i.e. $d\sigma = d\sigma^o (1 + \mathcal{P} \mathcal{A})$, with $d\sigma^o$ from Eq. (1) and \mathcal{A} the analyzing power. In the c.m. frame, three polarization states are observable [5, 6]: the longitudinal \mathcal{P}_z , the sideways \mathcal{P}_x , and the normal \mathcal{P}_y . The first two ones lie in the scattering plane, while the normal points in the $\mathbf{p}_1 \times \mathbf{k}_2$ direction, the

x, y, z , forming a right-handed coordinate system with the longitudinal z direction along the momentum of the outgoing proton. The \mathcal{P}_y is particularly interesting, since it is the only observable that does not require a polarization in the initial state [5, 6]. With the above approximations, it can be deduced by the spin asymmetry between events with positive and negative perpendicular polarizations:

$$\begin{aligned}\mathcal{P}_y &= \frac{1}{\mathcal{A}_y} \frac{d\sigma^\uparrow - d\sigma^\downarrow}{d\sigma^\uparrow + d\sigma^\downarrow} \\ &= \frac{b(q^2)}{2\sqrt{\tau-1} d\sigma^o} \sin \theta \left\{ \cos \theta \operatorname{Im} [G_M(q^2) G_E^*(q^2)] \right. \\ &\quad \left. - \sqrt{\frac{\tau-1}{\tau}} \operatorname{Im} [G_E(q^2) G_A^*(q^2, \cos \theta)] \right\}.\end{aligned}\quad (4)$$

This spin asymmetry is produced by the mechanism $\mathbf{p}_1 \times \mathbf{k}_2 \cdot \mathbf{S}_B$, which is forbidden in the Born approximation for the spacelike elastic scattering [6].

Measurements of the unpolarized distribution (1) and spin asymmetry (4) at fixed q^2 for different θ allow to fit the different angular terms, from which we may extract absolute values and relative phases of G_E/G_M , and some information on $G_A(q^2, \cos \theta)$. The Born contributions to $d\sigma^o$ and \mathcal{P}_y have a typical $\cos^2 \theta$ and $\sin 2\theta$ behaviours, respectively, any deviation due to non-Born terms. The normal \mathcal{P}_y vanishes at end points $\theta = 0, \pi$ and at threshold $q^2 = 4m^2(\tau = 1)$. Interestingly, at $\theta = \pi/2$ the Born contribution vanishes, and \mathcal{P}_y gives direct insight to the 2γ amplitude [16].

However, we note that the measurement of \mathcal{P}_y alone does not completely determine the phase difference of the complex form factors. By defining with δ_E and δ_M the phases of the electric and magnetic form factors, respectively, the Born contribution is proportional to $\sin(\delta_M - \delta_E)$, leaving the ambiguity between $(\delta_M - \delta_E)$ and $\pi - (\delta_M - \delta_E)$. Only the further measurement of \mathcal{P}_x can solve the problem, because $\mathcal{P}_x \propto \operatorname{Re}(G_M G_E^*) \propto \cos(\delta_M - \delta_E)$ [6]. But at the price of requiring a polarized electron beam.

III. GENERAL FEATURES OF THE NUMERICAL SIMULATIONS

We consider the $e^+e^- \rightarrow \vec{p}\bar{p}$ process. Most of the details of the simulation are mutuated from a previous work [15]. Therefore, events are generated in the usual variables q^2, θ, ϕ (the azimuthal angle of the proton momentum with respect to the scattering plane), and S_y (the proton polarization normal to the scattering plane). Then, the distribution is integrated

upon ϕ but not summed upon the spin.

The exchanged timelike q^2 is fixed by the beam energy. Only the scattering angle θ is randomly distributed. For a given q^2 , the Born terms in the unpolarized cross section (1) and spin asymmetry (4) are responsible for the $[1 + R(q^2) \cos^2 \theta]$ and $\sin 2\theta \operatorname{Im}[G_M(q^2) G_E^*(q^2)]$ behaviours, respectively. Since with the discussed approximations no other dependence in θ is present, observed systematic deviations from these behaviours will be interpreted as a clear signature of non-Born terms. The present lack of knowledge on such mechanisms forces us to further simplify the picture and to neglect the $\cos \theta$ dependence of the axial form factor by taking the first term of its expansion in powers of $\cos \theta$ (see Ref. [15] for further details).

An overall sample of 300 000 events has been considered with $3.8 \leq q^2 \leq 6.2 \text{ GeV}^2$ and $|\cos \theta| < 0.9$. We recall that the integrated cross section for $e^+e^- \rightarrow p\bar{p}$ in the considered region is approximately 1 nb; hence, at the foreseen luminosity of $10^{32} \text{ cm}^{-2}\text{s}^{-1}$ for DAFNE-2 [13, 14] this sample can be collected in one month with efficiency 1. The lower q^2 bin does not include the $p\bar{p}$ threshold, because this region is characterized by peculiar mechanisms like, e.g., the Coulomb focussing and possible subthreshold resonances. As it will be evident later, the spin asymmetry between events with positive and negative S_y polarization is very small for the first q^2 bin and would suggest to exclude it from the analysis. However, this would imply to reduce the size of the sample by almost a factor 2. In fact, the event distribution approximately falls like $1/q^{10}$ [15, 17], leaving the bins at higher q^2 scarcely populated. For more details, we refer to the discussion in Ref. [15]. Here, we just remark that the interesting quantities related to the spin asymmetry (4) increase approximately in a linear way from threshold to $q^2 \sim 5 - 6 \text{ GeV}^2$: while absolute errors increase with q^2 because of less populated bins, the relative errors do not (see discussion in Sec. V). Contrary to the unpolarized case, there is no reason to asymmetrically split the beam time in order to make the statistics of each q^2 bin more homogeneous. In any case, in the following we will use the "default conditions", as they were defined in Ref. [15]: the q^2 range is divided in 6 equally spaced bins with width $\Delta q^2 = 0.4 \text{ GeV}^2$; for each of them, the solid angle $|\cos \theta| < 0.9$ is divided in 7 equally spaced bins with width $\Delta \cos \theta \approx 0.257$. For each of the 42 bins, events are further divided according to their polarization, and the spin asymmetry is constructed according to Eq. (4) by taking the ratio between the difference and the sum of events with positive or negative polarization.

Events can be generated only by inserting specific parametrizations of the proton form factors in the cross section. For G_E and G_M , several models can be considered in the timelike region [4, 6], mostly derived from extrapolations from the spacelike region. As in Ref. [15], we select the parametrizations of Refs. [18, 19], because they have been recently updated in Ref. [4] by simultaneously fitting both the spacelike and timelike available data. Moreover, both cases release separate parametrizations for the real and imaginary parts of G_E and G_M , as they are needed in Eqs. (1) and (4). We indicate the former as the IJLW parametrization (from the initials of their authors), and the latter as the Lomon parametrization.

Since the explored q^2 range is not large, it is reasonable to make also much simpler, but equally effective, choices. In the previous work [15], we used parametrizations where all form factors are real and proportional to the same dipole term $1/(1+q^2/q_o^2)^2$, with $q_o^2 = 0.71 \text{ GeV}^2$, as in the spacelike region. The actual parameters were reduced to the ratios $r_e = |G_E/G_M|$ and $r_a = |G_A/G_M|$. However, this choice leads to a vanishing spin asymmetry, since all form factors have the same phase. Here, we generalize the case aiming to alternatively emphasize each one of the two contributions in Eq. (4), and analyze the conditions for their extraction. We define the parametrization Dip1*i* as the one with $r_e = 1$, $r_a = 0$, and where the relative phase of G_E with respect to G_M is $\beta_e = \pi/2$, i.e. both G_M and G_E have a dipole trend in q^2 but the former is real while the latter is purely imaginary; there are no effects from 2γ exchanges because $G_A = 0$. With Dip1*i*, only the Born term survives in Eq. (4) and its effect is maximized. The second choice is named Dip2*γi* and it is defined by $r_e = 1$, $r_a = 0.2$, and $\beta_e = 0$, $\beta_a = \pi/2$, with β_a the relative phase of G_A with respect to G_M . Namely, G_E and G_M are equal and real; G_A has the same dipole trend, but it is purely imaginary and with a modulus 5 times smaller than $|G_M|$. In this case, in Eq. (4) only the non-Born term is active and is maximized.

The Dip1*i* parametrization must not be considered realistic but rather an exercise to set the upper limit on $\text{Im}[G_E]$. In fact, for the considered q^2 range it is reasonable to expect $|G_E| \sim |G_M|$, since the two moduli are equal at threshold. Moreover, $\text{Im}[G_E]$ cannot be large considering that the absorption induced by the $p - \bar{p}$ rescatterings is much below the unitarity limit (see Ref. [15], and references therein). Indeed, the Born contribution to the asymmetry induced by the Lomon parametrization, turns out to be not larger than 10%; at these q^2 , the IJLW parametrization gives even a vanishing asymmetry. On the other side, we notice that nothing can be presently said about the relative weight of $\text{Re}[G_A]$ and

$\text{Im}[G_A]$. If for the considered q^2 range we can approximately take $\text{Im}[G_{E/M}] \sim 0$, we deduce from Eq. (1) that the $\text{Re}[G_A]$ can be best extracted from the unpolarized reaction and it was analyzed in Ref. [15]. Viceversa, the assumption in $\text{Dip}2\gamma i$ of a large $\text{Im}[G_A]$ selects the normal polarization of Eq. (4) as the best observable to study 2γ exchanges. In this sense, the choice $\text{Dip}2\gamma i$ is also an attempt to set a possible upper limit to non-Born contributions. However, as in Ref. [15] we stress that we set $r_a = |G_A|/|G_M| = 0.2$ to account for these effects as corrections to the Born result. In particular, we note that a correction of 20% does not contradict the experimental findings on G_E/G_M in the spacelike region with the polarization transfer method [2].

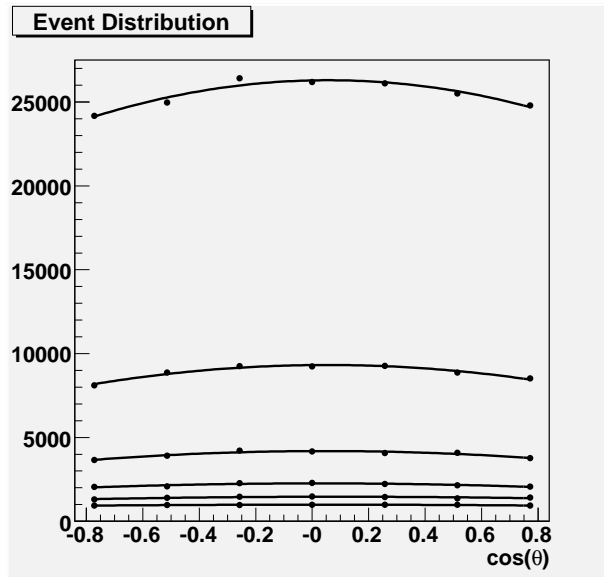


Figure 1: Angular distribution of 300 000 events for the $e^+e^- \rightarrow p\bar{p}$ process at $3.8 \leq q^2 \leq 6.2$ GeV^2 and $|\cos \theta| < 0.9$, and with the Lomon parametrization of proton form factors (see text). The points correspond to 7 equally spaced $\cos \theta$ bins for each of 6 equally spaced q^2 bins. Solid curves are the results of a 3 parameters angular fit with $B \propto r_a = |G_A/G_M| = 0$ (see text). The highest curve corresponds to the lowest bin $3.8 \leq q^2 \leq 4.2$ GeV^2 ; next lower curve to the adjacent bin $4.2 \leq q^2 \leq 4.6$ GeV^2 , and so on.

IV. RECONSTRUCTION OF THE SPIN ASYMMETRY

In Ref. [15], we analyzed in detail the conditions for an unpolarized $e^+e^- \rightarrow p\bar{p}$ measurement at DAFNE-2 [13, 14] in order to estimate the achievable precision in the reconstruction

of $r_e = |G_E/G_M|$ and in a possible detection of 2γ contributions. As it has been recalled in Sec. I, the complete determination of G_E and G_M in the timelike region requires the knowledge of their relative phase, which in turn involves the polarized $e^+e^- \rightarrow \vec{p}\bar{p}$ measurement.

Our analysis consists of five steps. For sake of simplicity, we describe it in the following for the case of the Lomon parametrization:

- 1) We generate 300 000 events for $3.8 \leq q^2 \leq 6.2$ GeV 2 and $|\cos \theta| < 0.9$ (i.e., for $25^\circ \leq \theta \leq 155^\circ$). The sorted events are summed upon the positive and negative polarizations S_y and are divided into 6 equally spaced q^2 bins of width $\Delta q^2 = 0.4$ GeV 2 . In each q^2 bin, the events are divided into 7 equally spaced $\cos \theta$ bins with width $\Delta \cos \theta \approx 0.257$. In Fig. 1, the points show the 6 unpolarized distributions in q^2 , each one consisting of 7 points describing the distribution in $\cos \theta$. From the discussion in the previous section, the highest $\cos \theta$ distribution corresponds to the lowest bin $3.8 \leq q^2 \leq 4.2$ GeV 2 ; the next lower distribution to the adjacent bin $4.2 \leq q^2 \leq 4.6$ GeV 2 , and so on.
- 2) For each q^2 bin, the $\cos \theta$ dependence of the unpolarized event distribution is fitted by a function of the form

$$C_q(\cos \theta) \equiv A N_q(\cos \theta) = A(1 + R \cos^2 \theta - B \cos \theta), \quad (5)$$

where the three fitting parameters A , R , and B , change for each different q^2 bin. The results of each fit are represented by the solid curves in Fig. 1. The parameter A is related to the total number of collected events and it does not play any role in the following analysis; R is connected to the angular coefficient $R(q^2)$ of Eq. (3), and B to the correction from 2γ exchanges (for a thorough discussion, see Ref. [15]).

- 3) For each q^2, θ bin, the events generated at step 1) are divided in two groups corresponding to positive (U) and negative (D) normal polarizations S_y . Then, the spin asymmetry is manually constructed by taking the ratio $(U - D)/(U + D)$. In Fig. 2, the full squares show the $\cos \theta$ distribution for the lowest q^2 bin, while the empty squares refer to the largest q^2 bin.
- 4) After fixing $N_q(\cos \theta)$, for each q^2 bin the θ dependence of the spin asymmetry is fitted

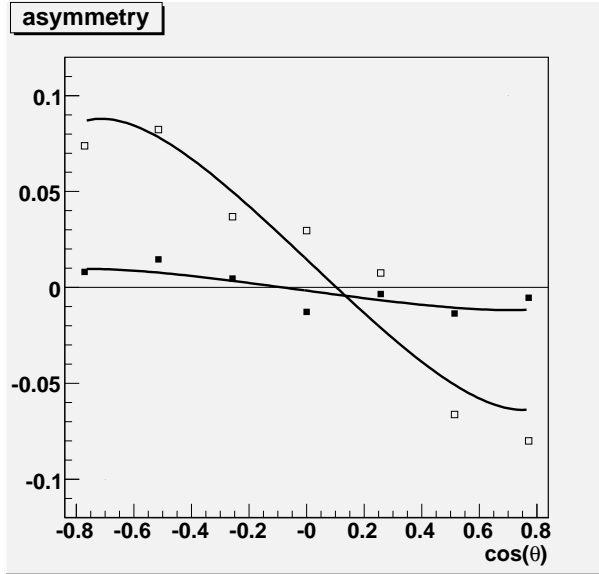


Figure 2: Normal polarization for the $e^+e^- \rightarrow \vec{p}\bar{p}$ process in the same conditions as in Fig. 1. Full squares refer to the lowest bin $3.8 \leq q^2 \leq 4.2 \text{ GeV}^2$, empty squares to the highest $5.8 \leq q^2 \leq 6.2 \text{ GeV}^2$. Solid lines are the result of a 2 parameter angular fit (see text).

by a function of the form

$$A_q(\theta) = \frac{\sin \theta}{N_q(\cos \theta)} (A_1 \cos \theta - A_2) , \quad (6)$$

where the fit parameters A_1 and A_2 refer, respectively, to the Born term $\text{Im}[G_M G_E^*]$ and to the non-Born term $\text{Im}[G_E G_A^*]$ in Eq. (4). The results of the fits for the lowest and largest q^2 bins are represented by the solid lines in Fig. 2.

- 5) The procedure is repeated 10 times, starting from statistically independent samples, and average values and statistical variances for A_1 and A_2 are built for each q^2 bin and displayed in Fig. 3. We checked that stability of the results is ensured already after 6 repetitions. In the figure, each point is accompanied also by two other error bars, whose meaning is the following. For each repetition, A_1 and A_2 are determined with some error from the fitting procedure. From left to right, the second error bar associated to each point is the average of the fitting errors upon the 10 repetitions. We recall that this error gives the integral deviation of the test function from the data points; therefore, it must be considered as a systematic error and, in principle, it has nothing to do with the statistical one. Finally, the rightmost error bar associated to each point gives the uncertainty on A_1 and A_2 deriving from the uncertainty on

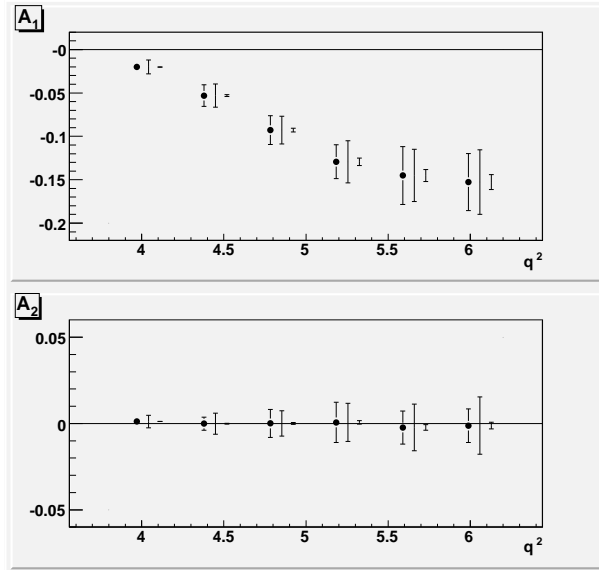


Figure 3: Values of the fitting parameters A_1 and A_2 extracted from the normal polarization of Fig. 2 according to Eq. (6). For each point, the leftmost error bar gives the statistical error, the central error bar gives the fitting (systematic) error, the rightmost error bar is the uncertainty associated with the fitting error on the unpolarized event distribution.

the separately fitted parameters R and B : when the latter ones oscillate between the extreme values allowed by their fitting error bars, the averages values of A_1 and A_2 can oscillate inside the rightmost error bars displayed in Fig. 3.

The Lomon parametrization includes only Born contributions to the complex G_E and G_M , i.e. $G_A = 0$ in Eqs. (1) and (4). Consequently, the unpolarized angular distributions of Fig. 1 are symmetric functions in $\cos\theta$ and the spin asymmetry of Fig. 2 displays the typical $\sin 2\theta$ trend, as it should be. Consistently, the fit parameter A_2 , related to the interference between G_A and G_E , turns out to vanish in Fig. 3 within the statistical (and fitting) uncertainty.

The fits of the unpolarized distribution and of the spin asymmetry are separately performed, because each single generated event can be collected in the group with positive (U) or negative (D) normal polarization, defining the asymmetry as $(U - D)/(U + D)$. Our procedure corresponds to separately fit the denominator $U + D$ (with the 3 fit parameters A, R , and B) and the numerator $U - D$ (with the 2 fit parameters A_1 and A_2). The uncertainty in the former fitting procedure does not affect much the latter one. This can be

visualized by the rightmost error bar associated with each point in Fig. 3. We checked that this is not accidental by repeating the fit of the spin asymmetry but artificially assuming the denominator $U + D$ independent from $\cos\theta$: the results on A_1 and A_2 stay basically the same. It must be noted, however, that in the considered q^2 range both the angular coefficient $R(q^2)$ of Eq. (3) and the non-Born contribution proportional to $\text{Im}[G_M G_A^*]$ are small, because $|G_E| \approx |G_M|$ and G_A is assumed to vanish in the Lomon parametrization. In general, for larger q^2 the first condition may not be satisfied, while the second one appears too drastic. Consequently, the analysis of error bars would become more involved; but a discussion along this line is beyond the scope of this paper.

As previously described, the first and second leftmost error bars in Fig. 3 represent the statistical and fitting errors on A_1 and A_2 . The fitting error is usually a systematic error, except in those situations where in the limit of a large number of events the test function reproduces exactly the event distribution. This may happen when the number of fit parameters is equal to the number of bins (which is not our case, because we have 2 parameters against 7 bins in $\cos\theta$), or when the test function is the correct guess for the event distribution. In general, this is not possible since, in reality, the θ dependence of the form factors is unknown. But this is the case of our simulation, where we have neglected the θ dependence in all form factors and the fitting functions (5) and (6) reproduce the complete angular dependence of the event distributions. Therefore, in the limit of a large number of events the statistical and fitting errors become equal; for the 300 000 events considered here, they are very similar, as it is evident from Fig. 3. The main consequence is that, in the conditions previously discussed, the statistical and fitting errors are two different ways to estimate the same error, and they must not be summed as one usually does for statistical and systematic errors. This statement can be safely generalized when the analysis is performed in the Born approximation, because G_E and G_M depend only on q^2 and the fitting functions (5) and (6) with $B = 0$ and $A_2 = 0$, respectively, are certainly correct. It is more questionable when non-Born contributions are included, either in $G_{E/M}$ or via G_A , and the $\cos\theta$ dependence should be considered also inside the form factors.

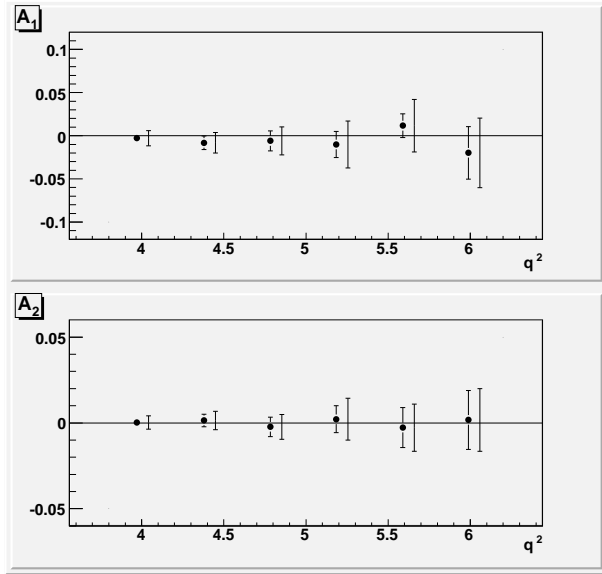


Figure 4: The same as in Fig. 3, but for the IJLW parametrization (the rightmost error bar for each point is not displayed).

V. DISCUSSION OF RESULTS

In the following, we discuss the output of repeating the procedure outlined in the previous section but for different parametrizations, as they have been described in Sec. III. For sake of brevity, we will omit the figures with the angular distributions and will show only the dependence on q^2 of the parameters A_1 and A_2 extracted from the fit. For each point, only the statistical and fitting errors will be displayed, since the sensitivity to the uncertainty on the R and B parameters of Eq. (5) is small (see Fig. 3).

In Fig. 4, the average values of A_1 and A_2 with statistical and fitting errors are displayed for the considered q^2 bins for the IJLW parametrization. The A_2 is consistently compatible with zero because no 2γ effects are included. Surprisingly, the A_1 is also compatible with zero, while at much larger q^2 this choice gives very large asymmetries, similarly to the Lomon parametrization [4]. Luckily, the relatively small error bars allow to unambiguously distinguish the two realistic parametrizations, except maybe for the lowest q^2 bin.

It is not accidental that the cleanest comparison is possible for the largest q^2 here considered. At the threshold $q_{th}^2 = 4m^2$, we have $G_E = G_M$ and the Born term in Eq. (4) vanishes. For q^2 not much larger than q_{th}^2 , we may assume that

$$G_E \approx G_M \left[1 - \alpha (q^2 - q_{th}^2) + \dots \right] e^{i[\beta (q^2 - q_{th}^2) + \dots]} . \quad (7)$$

The Born term of the spin asymmetry will behave like $-\sin[\beta(q^2 - q_{th}^2)] [1 - \alpha(q^2 - q_{th}^2)] \approx -\beta(q^2 - q_{th}^2)$ for small $q^2 - q_{th}^2$. Hence, it is easy to justify the approximate linear dependence for $q^2 \leq 5 \text{ GeV}^2$ displayed both in Fig. 3 and Fig. 4.

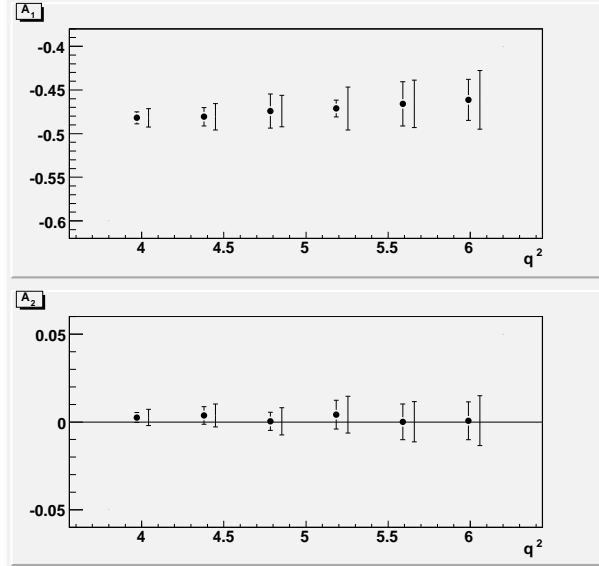


Figure 5: The same as in Fig. 3, but for the Dip1*i* parametrization (the rightmost error bar for each point is not displayed).

As anticipated in Sec. III, we have also considered the Dip1*i* parametrization which emphasizes the Born contribution to \mathcal{P}_y by taking $G_A = 0$ and G_E purely imaginary with the same modulus as G_M . The corresponding fit parameters A_1 and A_2 are displayed in Fig. 5: A_2 is obviously consistent with zero, while A_1 is roughly three times larger in size than in the more realistic parametrizations Lomon and ILJW. Evidently, it must be considered as an upper limit.

Similarly, the parametrization Dip2 γ *i* emphasizes the non-Born contribution in \mathcal{P}_y by taking G_E and G_M real and G_A purely imaginary. As already discussed in Sec. III, this is not an upper limit for the 2γ effects, since we have imposed $|G_A|/|G_M| = 0.2$, consistently with the findings in the spacelike region about the G_E/G_M ratio [2]. But it represents the most favourable situation to explore $\text{Im}[G_A]$ using the spin asymmetry. In Fig. 6, A_1 is obviously consistent with zero, and A_2 indicates a clearly detectable effect.

Analogously to the Born case, the 2γ effects seem better visible at the largest q^2 here explored, even if the latter correspond to the least populated bins. We note also that while the Born term in \mathcal{P}_y approximately falls like $|G_E/G_M|$ for increasing q^2 and, therefore, is not

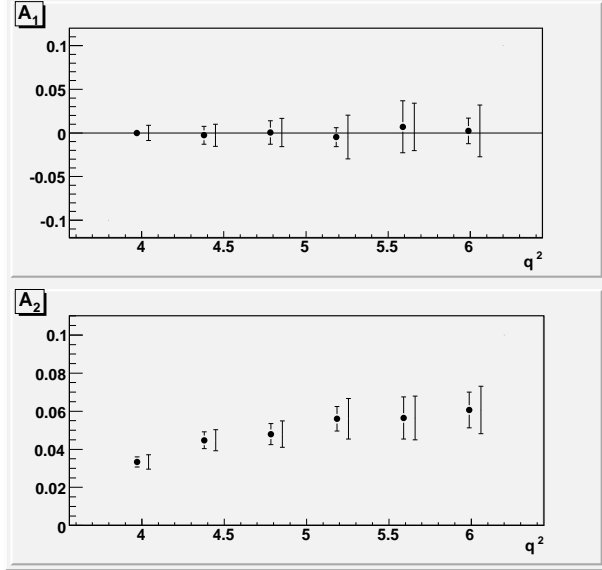


Figure 6: The same as in Fig. 3, but for the Dip2 γ i parametrization (the rightmost error bar for each point is not displayed).

expected to fall fastly unless far beyond 10 GeV² [9], viceversa, from Eq. (4) together with Eqs. (1,2), the weight of the 2 γ contribution should fall at least as $1/\sqrt{\tau} \sim 1/q$. Therefore, unless the 2 γ effect increases with q^2 , the available range of its measurability is reduced to $q^2 < 10$ GeV².

VI. CONCLUSIONS

We have performed numerical simulations of the single-polarized $e^+e^- \rightarrow \vec{p} \bar{p}$ process using a sample of 300 000 events in the kinematical region with $3.8 \leq q^2 \leq 6.2$ GeV², distributed over 6 equally spaced bins. For each q^2 bin, event have been further distributed over 7 equally spaced bins in $\cos(\theta)$, with $|\cos \theta| < 0.9$. For each q^2, θ bin, the events have been separated in two groups according to their positive (U) or negative (D) normal polarization of the recoil proton with respect to the reaction plane.

The angular distributions of $U + D$ (the unpolarized cross section) has been fitted with a three-parameter function of the type $A[1 + R \cos^2 \theta - B \cos \theta]$, where from the parameters R and B information on $r_e = |G_E/G_M|$ and $r_a = |G_A/G_M|$ can be deduced, respectively. The angular distribution $U - D$ (proportional to the spin asymmetry) has been fitted with the two-parameter function $\sin \theta [A_1 \cos \theta - A_2]$, where the two free parameters A_1 and A_2 are

related to $\text{Im}[G_M G_E^*]$ and $\text{Im}[G_E G_A^*]$, respectively, i.e. to the relative phases of the complex form factors.

Using realistic parametrizations for G_E and G_M deduced by fitting the available spacelike and timelike data, the statistical uncertainty makes it possible to unambiguously distinguish among different models, which are equivalent in the spacelike domain. Therefore, both moduli and phases can be extracted with a two-step fitting procedure, where the fitting errors of the first step do not affect much the uncertainty in the second step. Surprisingly, the extraction of phases seems better performed for the higher q^2 bins, because the spin asymmetry is small for q^2 close to the threshold and the relative error becomes smaller and smaller for increasing q^2 .

The additional contribution related to two-photon exchange diagrams shows up as a deviation from the expected angular trend of the Born contribution, via the parameters B and A_2 . In our analysis, we modeled such contribution in terms of the complex axial form factor G_A , constraining its modulus not to contradict the findings in the spacelike region. Nothing can be said about the relative weight of $\text{Re}[G_A]$ and $\text{Im}[G_A]$. However, assuming that for the considered q^2 range G_E and G_M are similar and with small imaginary parts, information on $\text{Re}[G_A]$ and $\text{Im}[G_A]$ can be extracted from the non-Born term of the unpolarized cross section and of the spin asymmetry, respectively. Using a simple dipole parametrization, our finding is that the non-Born term can be identified if its size is at least 5% of the Born contribution; if $\text{Im}[G_A]$ is the dominant term, the asymmetry related to the A_2 coefficient can be clearly measured, again with a preference for the highest q^2 bins.

Acknowledgements

The work of B.P. and M.R. is partially supported by the EU Integrated Infrastructure Initiative Hadron Physics under contract number RII3-CT-2004-506078.

[1] C.E. Hyde-Wright and K. De Jager, *Ann.Rev.Nuc.Part.Sci.* **54**, 217 (2004);
 H. Gao, *Int. J. Mod. Phys.* **E12**, 1 (2003) [Erratum-*ibid* **E12**, 567 (2003)];
 I.A. Qattan *et al.* [JLab Hall A], *Phys. Rev. Lett.* **94**, 142301 (2005).

[2] V. Punjabi *et al.* [JLab Hall A], Phys. Rev. C**71**, 055202 (2005) [Erratum-*ibid* **71**, 069902 (2005)];
 O. Gayou *et al.* [JLab Hall A], Phys. Rev. Lett. **88**, 092301 (2002);
 M.K. Jones *et al.* [JLab Hall A], Phys. Rev. Lett. **84**, 1398 (2000).

[3] A.V. Afanasev *et al.*, Phys. Rev. D**72**, 013008 (2005);
 P.G. Blunden, W. Melnitchouk, and J.A. Tjon, Phys. Rev. C**72**, 034612 (2005);
 M.P. Rekalo and E. Tomasi-Gustafsson, Eur. Phys. J. A**22**, 331 (2004).

[4] E. Tomasi-Gustafsson *et al.*, E. Phys. J. A**24**, 419 (2005).

[5] A.Z. Dubnickova, S. Dubnicka, and M.P. Rekalo, Nuovo Cimento A**109**, 241 (1996).

[6] S.J. Brodksy *et al.*, Phys. Rev. D**69**, 054022 (2004).

[7] P. Mergell, U.-G. Meissner, and D. Drechsel, Nucl. Phys. A**596**, 367 (1996);
 H.-W. Hammer, U.-G. Meissner, and D. Drechsel, Phys. Lett. B**385**, 343 (1996).

[8] M. Andreotti *et al.* [E685], Phys. Lett. B**559**, 20 (2003).

[9] B. Aubert *et al.* [BaBar], Phys. Rev. D**73**, 012005 (2006).

[10] B. Bardin *et al.* [LEAR], Nucl. Phys. B**411**, 3 (1994).

[11] A. Antonelli *et al.* [FENICE], Nucl. Phys. B**517**, 3 (1998).

[12] R. Baldini *et al.*, Eur. Phys. J. C**11**, 709 (1999).

[13] N. Apokov *et al.*, *Measurement of the Nucleon Form Factors in the Time-Like region at DAFNE*,
 Letter of Intent (October 2005), see http://www.lnf.infn.it/conference/nucleon05/loi_06.pdf

[14] F. Ambrosino *et al.*, *Prospects for e^+e^- physics at Frascati between the ϕ and the ψ* ,
 hep-ex/0603056.

[15] A. Bianconi, B. Pasquini, and M. Radici, Phys. Rev. D**74**, 034009 (2006).

[16] G.I. Gakh and E. Tomasi-Gustafsson, Nucl. Phys. A**771**, 169 (2006).

[17] S.J. Brodsky and G.P. Lepage, Phys. Rev. D**24**, 2848 (1981).

[18] F. Iachello, A.D. Jackson, and A. Lande, Phys. Lett. B**43**, 191 (1973);
 F. Iachello and Q. Wan, Phys. Rev. C**69**, 055204 (2004).

[19] E.L. Lomon, Phys. Rev. C**66**, 045501 (2002).